Agricultural and Forest Meteorology 308-309 (2021) 108529

Contents lists available at ScienceDirect

Agricultural and Forest Meteorology

journal homepage: www.elsevier.com/locate/agrformet

Surface energy balance and flux partitioning of annual crops in southwestern France

Oluwakemi Dare-Idowu [a,*], Aurore Brut [a], Joan Cuxart [b], Tiphaine Tallec [a], Vincent Rivalland [a], Bartosz Zawilski [a], Eric Ceschia [a], Lionel Jarlan [a]

[a] CESBIO, Université de Toulouse, CNES/CNRS/INRAE/IRD/UPS, Toulouse, France
[b] University of the Balearic Islands, Palma, Mallorca, Spain

ARTICLE INFO

Keywords:
Surface energy balance
Eddy covariance
Flux partitioning
Advection

ABSTRACT

In the micrometeorology community, it is well known that the turbulent fluxes measured with eddy covariance (EC) systems do not usually equal the available energy. Hence, qualitative knowledge of the impact of different vegetation types, and climatic variables on this 'nonclosure' is essential. This study analyzed a unique database of EC flux measurements covering 8 growing seasons of 3 crops (maize, wheat, and rapeseed) cultivated over two close agricultural sites (FR-Lam and FR-Aur) in southwestern France. For data analysis, some dry and wet cropping seasons of the same crop type were selected; then, their phenological stages were identified to investigate their effect on the energy balance closure (EBC), and flux partitioning. The results showed that the systematic effect of each site on the EBC was stronger than the influence of crop type and stage, as EBC was generally higher at FR-Aur (82%) than at FR-Lam (67%), even for the same crop type. The assessed effect of rainfall, and phenological stages on energy partitioning revealed that during the wet seasons, over 42% of the net radiation (*Rn*) was accounted for by the latent heat flux (*LE*), which was 9% higher than the recorded *LE* in the dry year during the active vegetation period. Similarly, the ground heat flux (*G*) was observed to be very sensitive to vegetation; *G* accounted for 30% of *Rn* when vegetation was low, whereas at the peak of vegetation, it fell below 16% due to canopy shading. Closure was also assessed under various atmospheric stability conditions and wind sectors, and it was observed to be higher under unstable conditions, and in prevailing wind directions. Analysis of the sensible heat advection (A_H) revealed that A_H accounts for more than half of the imbalance at both sites.

1. Introduction

Since the publication of Foken and Oncley (1995) that highlighted both the limitations encountered in the direct measurement of turbulent fluxes, and propositions on how to address this "unclosed" energy budget in the atmospheric surface layer, there have been numerous experimental studies (beginning with Panin et al., 1998; Laubach and Teichmann, 1999) aimed at the surface energy balance (SEB) problem. The SEB is an extension of the first law of thermodynamics that is applied to a conceptual budget volume across the atmosphere-surface continuum. The traditional expression of this concept given in Eq. (1) requires that the total available energy (*Rn-G*), where *Rn* is the net radiation and *G* is the ground heat flux, should be equal to the sum of the sensible heat flux (*H*), and latent heat flux (*LE*) (Foken, 2008; Mauder et al., 2020). However, this simplified representation does not fully match what is experimentally measured, and it results in the so-called energy balance closure problem.

$$Rn - -G = LE + H \quad (1)$$

Over the years, several propositions have been put forward to explain the possible causes of this nonclosure with attempts to narrow the gap. Culf et al. (2004) highlighted measurement errors as a key factor, especially the frequent maintenance required by net radiometers, as previously investigated by Field et al. (1992). This same factor was confirmed in Foken et al. (2008), and Aubinet et al. (2012), where it was added that energy imbalance is a scale problem; that is, the inability of the EC system to capture large-scale turbulent motions due to brief temporal resolutions. In support of the above, Leuning et al. (2012) pointed out that analysis of the half-hourly surface energy balance may be biased by inaccurate measurements of the storage terms, and

* Corresponding author.
E-mail address: dare.oluwakemi@cesbio.cnes.fr (O. Dare-Idowu).

https://doi.org/10.1016/j.agrformet.2021.108529
Received 25 October 2020; Received in revised form 14 June 2021; Accepted 24 June 2021
Available online 12 July 2021

questioned whether the energy balance is better closed at daily time scales since energy stored in the soil, air and biomass during the morning is released locally in the afternoon and evening.

Foken et al. (2010) found that around midday, more than 120 W m-^{2} of *Rn* was unaccounted for over a corn site even with high-quality data, which de-emphasized the significance of measurement errors and uncertainties. Similarly, Charuchittipan et al. (2014) found limited effect in increasing the averaging time on energy closure after applying both the block ensemble average and ogive analysis to measurements obtained during the LITFASS-2003 experiment. Their study suggested that a 30-min averaging time is sufficient over low vegetation for the modified ogive analysis, while a longer time scale is required for the block ensemble average.

Furthermore, Gao et al. (2017), who analyzed EC measurements over an irrigated cotton field during the EBEX campaign, hinted that the large residual energy (> 100 Wm^{-2}) is a result of the unrealistic requirements of the EC method, which solely suits homogeneous surfaces. In reality, most land surfaces are heterogeneous, e.g., heterogeneity introduced by cultivated crops at agricultural sites. Hence, this raises the question of how much imbalance is introduced by surface heterogeneity. Heterogeneity reinforces the 'different source areas' concept, which by itself reduces the ability to arrive at the satisfactory closure of '1′ due to short temporal measuring scales, and drawbacks of measuring methodologies. To quantify the impact of surrounding heterogeneities, Cuxart et al. (2016) estimated roughly the advection term (*A*) as a 'heterogeneity proxy' using 5 days of data over a small heterogeneous square of 1 km x 1 km during the BLLAST campaign. The study concluded that horizontal advection within hectometric scales significantly contributed to the energy imbalance, and this was later confirmed by a separate study in the campus of the University of the Balearic Islands, Spain (Garcia--Santos et al., V. 2018).

Still within this context, the impact that climatic variables and experimental set-up have on the energy balance closure (EBC) has been extensively studied. Indeed, the choice of either an enclosed or an open-path IRGA can largely affect the closure in some regions. For instance, Bagayoko et al. (2006) investigated the closure over a sorghum and a sheanut site in Kompienga, Burkina Faso (tropical region), for 4 contrasting seasons in order to understand the influence of rainfall on the degree of 'goodness' of the energy balance. Their results showed a 15% drop in the energy closure during the transitioning of dry to rainy season due to the high sensitivity of the Krypton Hygrometer to dirt, and to rainfall droplets.

To understand the influence of vegetation height on EBC, Masseroni et al. (2014) analyzed turbulent fluxes over a site in Livraga, Italy, and observed that storage terms became more significant with increasing vegetation height, which resulted in lower energy closure because storage terms are generally difficult to estimate accurately. Despite the application of several corrections to the flux data, an imbalance of ~25% persisted over this site (Livraga) even though a distance of 1.8 m was maintained between the EC system and the canopy top; this lies within the range of the recommended distance (1.5 - 2 m) above canopy top (Burba and Anderson, 2007). On the other hand, Baldocchi (1994), after analyzing the flux measurements that were simultaneously taken over closed wheat and open corn fields, found no major influence of crop type on the energy closure, but on the partitioning of the fluxes. *LE* measured over the wheat field was twice that measured over the corn field despite corn being a highly transpiring plant.

The above reviews evidently show that studies on crop growth stages over dynamic agricultural systems are rare. As a result, this study aims to understand the variability of the energy balance closure, and the flux partitioning using measurements obtained over two close agricultural sites.

This article is structured as follows: Section 2 provides a detailed description of the study sites, data sets, and employed methodologies. Section 3 assesses how the energy balance closure is impacted by the selected crops, their phenological stages, and some atmospheric variables. We then investigated how each phenological stage partitions the net energy, followed by the assessment of the significance of surface temperature heterogeneity on the energy balance closure. The succeeding sections discuss the results and conclusions.

2. Materials and methods

2.1. Site description with crop rotation

The two experimental sites (20 km apart) are located in southwestern France in the Occitanie region (see Fig. 1). They are part of the Regional Spatial Observatory (OSR), Zone Atelier Pyrénées-Garonne (ZA PYGAR), Critical Zone Observatories (OZCAR), and Integrated Carbon Observation System (ICOS) projects (Gaillardet et al., 2018).

2.1.1. Lamasquère site

Lamasquère (FR-Lam) (43°49′ N 1°23′ E) is a flat agricultural field owned by the Purpan Engineering School. It extends over 24 ha at an elevation of 180 m above sea level (a.s.l). FR-Lam is surrounded by a thick forest in the west, south, and eastern directions. This plot is characterized by a temperate climate with cold winters, rainy springs and autumns, and hot summer. The mean annual air temperature (T_a), cumulative rainfall (plus irrigation (P)), and mean wind speed (WS) are 13.3 °C, 629 mm, and 1.79 m s^{-1}, respectively. The dominant wind directions are to the West (W), Northwest (NW), and Southeast (SE), which correspond to the oceanic and regional Autan wind regimes. The soil composition is clay (54.3%), loam (33.7%), and sand (12%) (Béziat et al., 2009). The main rotational crops are winter wheat and irrigated maize, which are cultivated with mineral and organic fertilizer. Mustard was grown once as a winter cover crop in the autumn of 2013 (see Fig. 2a), and there was winter wheat regrowth in autumn 2011. At FR-Lam, the farmer usually plants wheat (Triticum aestivum L.) at the beginning of October, and harvests the crop in the following summer within the first two weeks of July. Wheat straw is also removed before deep tillage and plowing (a seedbed preparatory practice) for the sowing of maize (Zea mays L.) in the spring of the following cropping year. Maize is usually sown between April and mid-May, irrigated in phases over a 5-days period, and harvested green between mid-August and early September of the same year for livestock feeding.

2.1.2. Auradé site

Situated on hillsides with a 3% slope and in an open area, the Auradé site (FR-Aur) (43° 54′ N 1° 10′ E) is a 23.5 ha agricultural field situated at 245 m a.s.l. This slope (East-Northeast direction, down the slope) results in a 15 m height difference at some points which has significant impact on the wind properties. Dominated by stronger winds than FR-Lam, FR-Aur has an average recorded wind speed of 2.6 m s^{-1} with predominant winds in the west and east sectors. This site experiences a mean annual rainfall of 660 mm, with a mean annual temperature of 13.1 °C. The soil is mainly silty, with loam, clay, and sand contents of 47.1%, 32.3% and 20.6%, respectively. The crop rotation here is more diversified compared to FR-Lam. Wheat, barley, rapeseed and sunflower are frequently cultivated with mineral fertilization only (see Fig. 2). Plowing is not practiced, and tillage is very superficial (not deeper than 20 cm). Similar to FR-Lam, the winter crops (wheat and rapeseed) are sown in autumn and harvested in early July; the harvest residues are generally left on site for a while before being incorporated into the soil. Sunflower and barley were grown once in 2007 and 2015, respectively; hence, both crops were excluded from this study because they are not statistically representative.

2.2. In situ measurements

At both sites, meteorological variables, soil and vegetation parameters (leaf area index (*LAI*), crop height (*hveg*), and aboveground biomass (*ABG*)) are continuously monitored alongside agricultural practices. Table 1 summarizes the parameters used in this study, and their

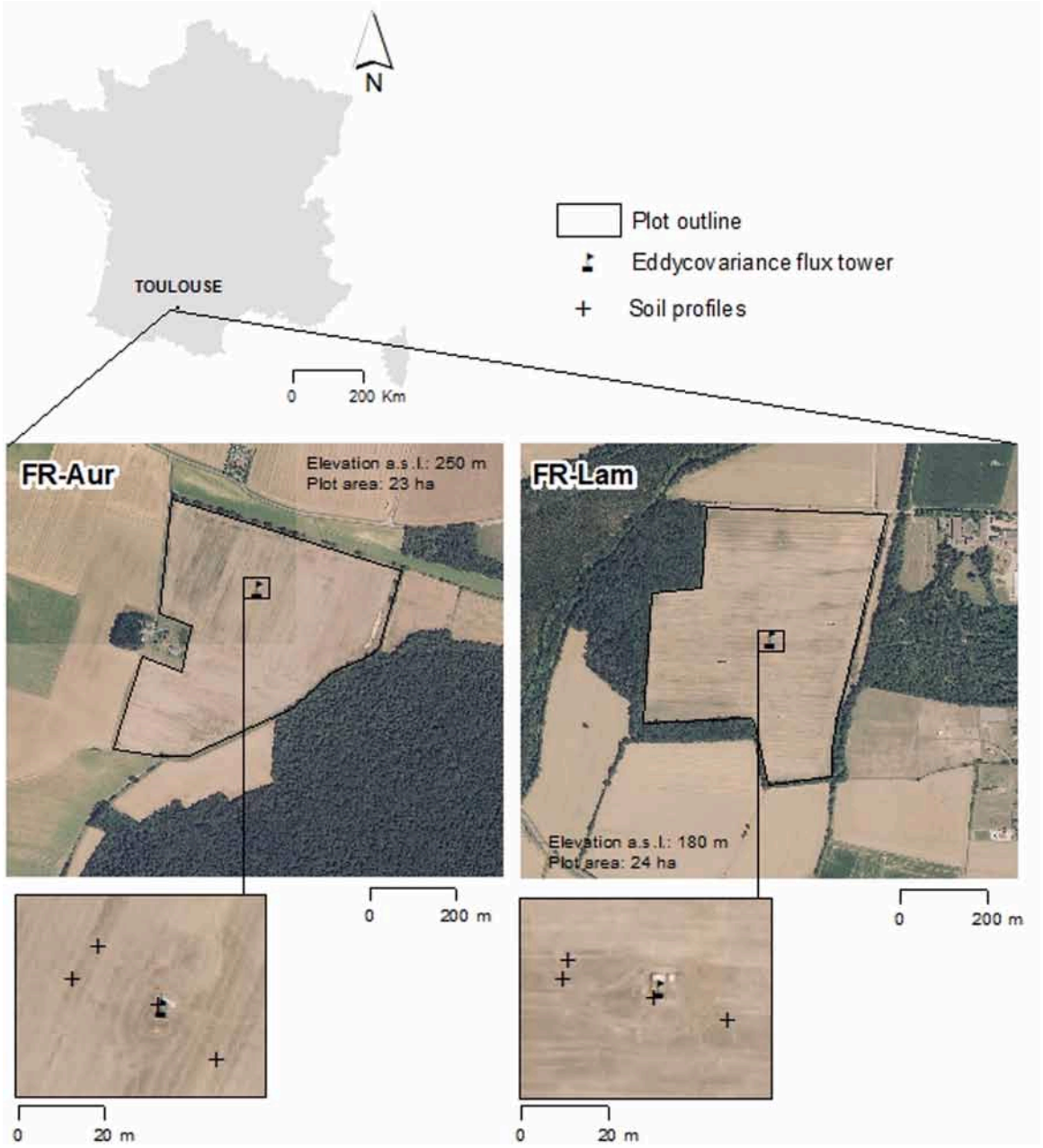

Fig. 1. Geographical location of the study sites in southwestern France (top). Experimental plots (middle) and setup location (bottom) of the EC system at the Aurade (left) and Lamasquère (right) site. Crosses represent the location of the pits where the temperature, the heat flux plates, and the soil water sensors are buried.

measuring instruments.

2.2.1. Meteorological, radiation and soil measurements

CNR1 (updated to CNR4 in 2012 with an overlap of several months) is a 4-component radiometer mounted on a dedicated mast that measures upwelling and downwelling radiation at a rate of 1 sample per min integrated over 30 min. The total spectral range incorporates wavelengths from 0.3 to 50 μm. Shortwave radiation (0.3 to 3.5 μm) is measured by two CM3 pyranometers: one measures the incoming solar radiation (*SWin*), while the other measures the reflected shortwave radiation (*SWout*). NRLite sensors were also installed at both sites between 2008 and 2012, and redundant measurements of incoming solar radiation were performed with SPN1 sensor from 2013.

The soil water content (*SWC*) was measured using reflectometer probes from 2005 to 2011 and then with a time domain reflectometer from 2012 to 2016 with 4 replicates located around the mast (see Fig. 1). Ground heat flux (G_z), which quantifies the energy transferred into the ground by conduction, is measured with 4 heat flux plates (HFPs) installed at a 5 cm depth inside the same pit where the *SWC* and temperature sensors are buried to obtain co-located measurements.

Some studies (McCaughy and Saxton, 1988; Eshonkulov et al., 2019) have identified storage terms as significant components of *Rn*, and Cuxart et al. (2015) suggests to treat all the non-explicitly accounted processes commonly in the imbalance term of the SEB; a term found to be of the same order of magnitude as the turbulent heat fluxes for an extensive vineyard in Spain. These terms represent (i) the energy stored between the top of the HFPs, and the surface of the soil (S_G), (ii) energy due to varying temperature/humidity within the canopy (H_{st}/L_{st}) and, (iii) the biochemical energy stored due to photosynthentic activities (S_p). S_G was computed in the top 5 cm of the soil using Eq. (2a) and Eq. (2b) taken from Campbell and Norman (1998).

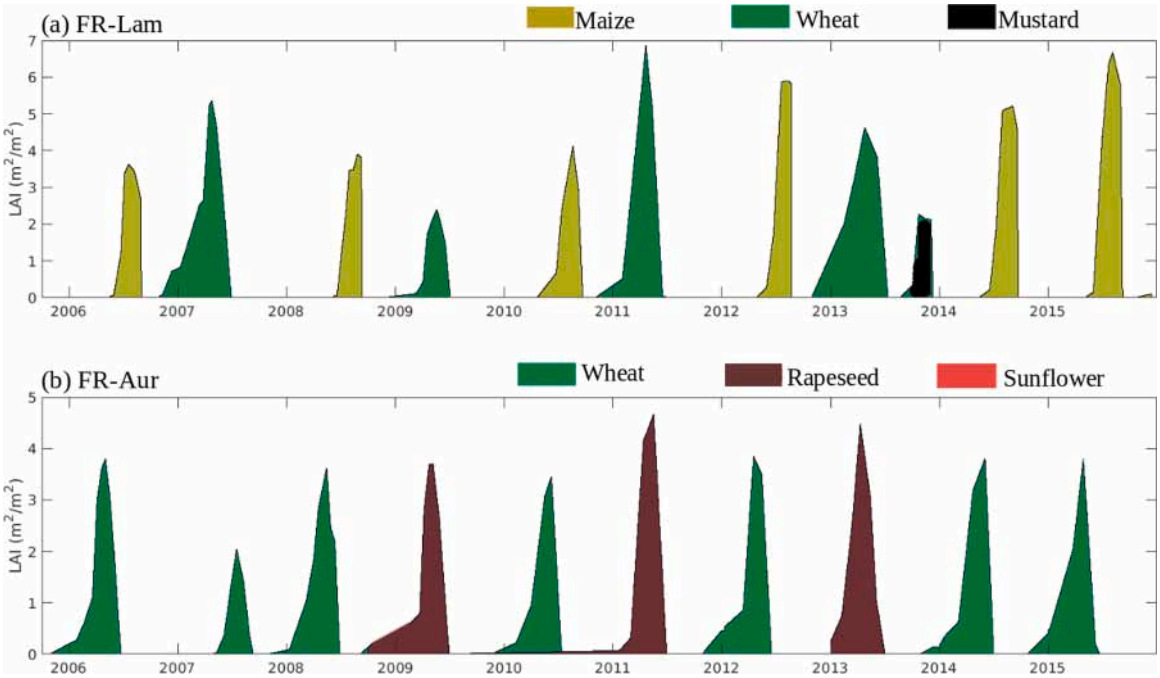

Fig. 2. Timeline and crop rotation at both sites from 2005 to 2016.

Table 1
Parameters and measuring instruments monitored at both sites at a half-hourly time step.

Parameter Description	Unit	Instrument (Vendor)
Wind speed & direction	m s^{-1} and °	Windvane (Young Prop) and WindSonic (Gill Ltd.)
A ir temperature & relative humidity	°C and %	HMP35 Temperature probe and Relative humidity sensor (VAISALA), VTP37 (MeteoLabor)
Leaf area index	m^2 m^{-2}	Planimeter
Soil moisture content (5 cm)	%	TDR/Theta Probe (ML2X, Delta-T)) and Reflectometer probes (CS616, Campbell Scientific)
Rainfall	mm	ARG100 Rain gage (Environmental Measurements Ltd.)
Ground heat flux at 5 cm depth	W m^{-2}	HFP01SC-L Heat Flux Plate (Hukseflux)
S oil temperature at 1, 5, 10, 30, 50 and 100 cm depth	°C	T107 Temperature Sensor (Campbell Sci.)
Net radiation, shortwave and longwave incoming and outgoing radiation	W m^{-2}	CNR1 and CNR4 Radiometer (Kipp & Zonen) NR lite radiometer (Kipp & Zonen); SPN1(Delta-T) for SW and diffuse radiation.
Turbulent fluxes (sensible heat and latent heat)	W m^{-2}	Eddy Covariance system (LI-7500 LI-COR Bio sciences + CSAT 3D- sonic anemometer from Campbell Scientific Ltd.)

$$S_G = \rho_s c_s \frac{dT}{dt} \tag{2a}$$

$$\rho_s c_s = \varphi_m \rho_m c_m + \theta \rho_m c_w + \varphi_0 \rho_0 c_0 \tag{2b}$$

where ρ_s is the soil density, c_s is the specific heat of the soil, T is the average temperature of the soil layer (calculated from soil temperature measurements at 0.05 m and 0.01 m depth), and t is the time. The volume calorimetric capacity of the soil ($\rho_s c_s$) was calculated from the fraction water volume of the layer, (θ was estimated by measuring the relative humidity of the soil at 0.05 m), and volume fractions of mineral (φ_m was estimated at 95%) and organic (φ_0 estimated at 5%). ρ_m, c_m, ρ_w, c_w, ρ_0, and c_0 represent respectively the density (2650 kg m^{-3}) and specific heat density (870 J kg^{-1} K^{-1}) of mineral matter, density (1000 kg m^{-3}) and specific heat density (4180 J kg^{-1} K^{-1}) of water, density (1300 kg m^{-3}) and specific heat density (1920 J kg^{-1} K^{-1}) of organic matter.

In parallel, H_{st} and L_{st} were calculated using Eq. (3a) and (3b) following Moderow et al. (2009), while S_p was estimated using Eq. (3c) following the approach proposed in Meyers and Hollinger (2004).

$$H_{st} = \int_0^z \rho_a(T_a) c_p \frac{\partial T_a}{\partial t} dz \tag{3a}$$

$$L_{st} = \int_0^z \lambda(T_a) \frac{\partial \rho_v}{\partial t} dz \tag{3b}$$

$$S_p = \alpha(GPP) \tag{3c}$$

where ρ_a is the air density (kg m^{-3}), T_a is the air temperature (K), c_p is the specific heat capacity of air at constant pressure (J kg^{-1} K^{-1}), and z represents the various measuring layers (0.5 m, 1.5 m, and 2 m in this study). Similarly, ρ_v is the vapor density of air, λ represents the latent heat of vaporization (J kg^{-1}), *GPP* is the gross primary productivity, and α is the equivalent solar energy used in CO_2 fixation, and it is approximately 422 kJ per mole of CO_2 fixed by photosynthesis (Nobel, 1974).

The estimation of the magnitude of these storage terms (see Fig. S1 and S2 in the Supplementary file) showed that the S_G is the most significant term; and when computed over daytime, an insignificant contribution from S_p (1.9% of *Rn*), L_{st} (0.09% of *Rn*), and H_{st} (0.37% of *Rn*) is observed. For the same time interval, S_G accounted for about 11% of *Rn*. Consequently, only S_G was considered in this study, as its magnitude sometimes approaches 60 W m^{-2} around midday during summer. For simplicity, the sum (G_z + S_G) is represented as G henceforth.

2.2.2. *Turbulent fluxes*

Exchanges of water vapor, energy, and carbon dioxide (CO_2) are measured continuously using the eddy covariance method. The EC system consists of (i) a 3D-sonic anemometer that measures the wind speed in three directions, as well as the sonic temperature of the air (to

calculate the air temperature), and (ii) an open path infrared gas analyzer that measures the CO_2 and water vapor density in the air at 20 Hz. These devices are mounted at heights of 2.8 m and 3.65 m at FR-Aur and FR-Lam, respectively. The EC towers are located at the center of each site to optimize the fetch in the main wind directions (see Fig. 1). *H* and *LE* fluxes were estimated according to Eq. (4a) and Eq. (4b).

$$H = \rho_a c_p \overline{w' T_a'} \quad (4a)$$

$$LE = \rho_a \lambda \overline{q' w'} \quad (4b)$$

where T_a', q' and w' are the deviations from the time averages of the air temperature (K), water vapor density (kg m^{-3}), and vertical wind speed (m s^{-1}), respectively (Nordbo et al., 2012). The overbars imply covariance over a defined averaging time. Half-hourly fluxes were calculated by post-processing the 20 Hz raw data according to the CarboEurope IP protocols (with the EdiRe Software). First, spikes due to both electronic and physical (rain for instance) noise were removed. Then, the fluxes were rotated (2D) in order to align the stream-wise velocity component with the direction of the mean wind vector. Besides, EC systems act as filters removing both high- and low-frequency components of the signal, and we applied Moore (1986) to correct the fluxes for spectral frequency loss. Eventually, water vapor fluxes were corrected for air density variations (Webb et al., 1980).

2.2.3. Quality check and data selection

Before using the data for the energy balance analysis, a data quality check was carried out, and this starts with a visual sorting of the time series. For *Rn*, the data from the best sensor, namely CNR4, then CNR1, and finally NRlite were selected. Moreover, for the overlapped periods between the different sensors measuring the net radiation, an intercomparison of these sensors made it possible to filter out data points that present a very strong dispersion around the regression line. In our case, a precision around 26 W m^{-2} is observed for net radiation, in agreement with Kohsiek et al. (2007).

We also performed a quality control of the eddy covariance measurements based on classical criteria. First, turbulent fluxes were discarded during rainfall periods according to Béziat et al. (2009). Meteorological conditions can also influence the requirements for EC measurements like steady state conditions, and a developed turbulent regime. Then, the stationarity test by Foken and Wichura (1996) was applied to EC fluxes in addition to the check proposed by Béziat et al. (2009) that only performs the steady state test when the absolute threshold between covariance over 30 min and means of covariances over 5 min for the corresponding half-hour was attained. Following the approach in Reichstein et al. (2005) that was adapted by Béziat et al. (2009) for crops, we used the friction velocity criteria combined with the crop functioning periods (CFP) to discard fluxes below the highest friction velocity threshold defined for each CFP. Eventually, a test on the footprint is performed (Kljun et al., 2004), and data points are discarded if less than 90% of the flux came from within the plot.

2.2.4. LANDSAT Land surface temperature

Launched in 1999 (2013), Landsat 7 (8) satellites continuously provided multi-spectral imageries of the Earth with one and two thermal bands, respectively. Hence, both satellites are rich sources of land surface temperature (*LST*) maps. From 2005 to 2015, *LST* maps (138 for FR-Lam) and (134 for FR-Aur) were retrieved from the Landsat 7 (ETM+) and Landsat 8 (OLI & TIRS) sensors at a high spatial resolution of 30 m at approximately 10h30, this time coincides with the passing time of the satellite over these stations (both stations were captured on the same scene). The retrieved thermal data were processed by the LANDARTs tool, and an extensive report of this processing technique has been well documented in Tardy et al. (2016). The acquired scenes were filtered by discarding scenes taken under cloudy conditions, and erroneous scenes with missing data due to SLC-off on Landsat 7 (a mechanical failure of the scan line corrector since 2003). From the 71 scenes retained for FR-Lam and the 52 for FR-Aur, *LST* data were retrieved as geo-located digital values and then corrected for atmospheric and surface emissivity effects using the LANDARTs tool. These retrieved values are used to estimate both spatial, and temporal temperature variability (ΔT in Eq. (5)) over FR-Lam and FR-Aur by adopting the methodology developed in Cuxart et al. (2016). Even though Landsat *LST* values were used instead of the ground *LST* (estimated from the Stefan-Boltzmann relationship), possible errors were minimized because only the temperature gradient (ΔT) was considered.

2.3. Methodology

This study was conducted in a comparative way between dry crop-seasons (low rainfall) and wet crop-seasons (high rainfall) in order to assess the controlling effect of rainfall, and the resulting soil moisture on the EBC. To this end, we first selected crop seasons with contrasting rainfall amounts (irrigation inclusive) at each site for each crop type. A crop season spanned from 2 weeks after seed germination up until the bare soil phase.

2.3.1. Contrasting crop-seasons

Table 2 *P* in mm is the cumulative rainfall (+irrigation for maize), and T_a in °C is the mean air temperature during each crop season. The 'timeline' column highlights the duration of each crop season, while 'nos' represents the number of days for each timeline.

2.3.2. Characterization of the phenological stages of selected crop-seasons

Five (four for maize) distinct periods for each selected crop were defined as follows; and abbreviations used in the figures are shown in the parenthesis: (i) Low crop: a period between 2 weeks after seed germination until $h_{max}/2$, where h_{max} is the maximum height attained by the crop. (ii) Developed crop (Dev crop): this period spans from $h_{max}/2$ until the initiation of senescence. (iii) Senescent crop (Senc crop): this runs from the end of a developed crop phase until the harvest day with the exception of maize where the plants were harvested green, (iv) Postharvest (Post hrv): this phase spans the period between the harvest day, and the soil work (harvest residues are present), and (v) Bare-soil: this period represents the seedbed preparation for the next planting season. For a pair of contrasting seasons, each crop stage had comparable data size to prevent bias.

2.3.3. Advection term

Considering topographical heterogeneity, while minding uneven canopy strength and resistance, the sensible heat advection term (A_H), which is taken as a surface temperature heterogeneity proxy, was estimated using the expression in Eq. (5).

$$A_H = \rho_a C_p z U \frac{\Delta T}{\Delta x} \quad (5)$$

where ρ_a is the air density, C_p is the specific heat capacity of air at constant pressure, z is the measuring height of the EC system, *U* is the average wind speed of the prevailing wind during the measuring period (m s^{-1}), and $\Delta T/\Delta x$ is the temperature gradient (from the EC systems to the reference point whose varying position depends on the direction of the prevailing wind) over a fixed distance ($\Delta x = 400$ m) from the EC system. A hectometer scale of 400 m was used because a larger or smaller scale would result in advection values that would be too small to be significant or too large to be meaningful, which would not be a good representation of the sites' footprint. Vertical advection was ignored in this study based on the simplification proposed by Cuxart et al. (2016), while the latent heat advection term (A_{LE}) was also left unaddressed since it would require a network of moisture sensors, and this is currently unavailable.

Table 2
presents the breakdown of the contrasting crop-seasons using rainfall amount as a proxy. For the same crop at each site, two dissimilar seasons were compared such that the difference between their cumulative rainfalls exceeded 100 mm.

FR-Lam					FR-Aur				
	P	T_a	Timeline	nos		P	T_a	Timeline	nos
Maize dry	338	19.7	04/06/2008 - 30/11/2008	176	Rapeseed dry	425	13.4	18/11/2010 - 16/10/2011	328
Maize wet	447	18.6	11/05/2012 - 05/11/2012	176	Rapeseed wet	773	12.3	01/11/2012 - 30/09/2013	329
Wheat dry	564	12.6	09/11/2010 - 13/01/2012	426	Wheat dry	416	13.6	24/12/2005 - 05/09/2006	251
Wheat wet	693	11.7	31/10/2006 - 04/01/2008	426	Wheat wet	580	14.3	08/01/2014 - 19/09/2014	249

3. Results and discussion

3.1. Overview of the energy balance closure

Two parameters were defined as EBC proxies. First, the sum of turbulent fluxes (H+LE) was plotted against the available energy (Rn-G) at a half-hourly time step; the slope of the linear fit corresponds to the EBC. A closed budget is associated with a straight line with a slope of 1 and an ordinate at the origin of 0. Secondly, the residual energy computed as $Res = Rn\text{-}G\text{-}H\text{-}LE$ corresponds to the missing energy in W m^{-2}.

Fig. 3 shows the variability in the closure of the contrasting crop-seasons using half-hourly fluxes. Higher EBCs ranging from 0.78 to 0.94 were observed at FR-Aur, while closure did not exceed 0.71 at FR-Lam. Closure was 18% and 20% higher for wheat-Lam and rapeseed-Aur, respectively, during the dry seasons than during the wet seasons. Similarly, the intercepts for these dry seasons were smaller, indicating smaller systematic errors. For the other crop-seasons, a contrasting behavior was observed; EBC was much lower in the dry year, and with a lower R^2. These findings imply an unclear effect of rainfall on the EBC, which could be because there is rarely water shortage at both sites. FR-Lam is located in the proximity of the river Le Touch, and presents a shallow water table, while at FR-Aur the rainfall is much higher, and crops are often sown between Autumn, and the beginning of winter. Similarly, the large difference between the average EBC recorded for wheat at FR-Lam (0.65) and wheat at FR-Aur (0.89) implies that the crop type had no significant effect on EBC; rather, closure was strongly dependent on site characteristics.

3.2. Dependency on atmospheric parameters

3.2.1. Wind direction

The SEB is studied as a function of wind direction, and therefore depends on spatially different turbulent flux footprints. Supposing that the surfaces are homogeneous, they should exchange the same fluxes whatever the direction, and the closure should be identical. Flux measurements of these selected crops were categorized into 8 classes; each class corresponds to the following wind directions: North-N ($\theta < 22.5°$ & $\theta >= 337.5°$), Northeast-NE ($22.5° <= \theta < 67.5°$), East-E ($67.5° <= \theta < 112.5°$), South-S ($155.5° <= \theta < 202.5°$), Southeast-SE ($202.5° <= \theta < 225.5°$), Southwest-SW ($225.5° <= \theta < 247.5°$), West-W ($247.5° <= \theta < 292.5°$), and Northwest-NW ($292.5° <= \theta < 337.5°$). The energy balance closure of each group was estimated as presented in Fig. 4. The size of the dot represents the number of samples (which is smaller for maize because of the short life cycle), and the color corresponds to the EBC value. The main wind directions at the FR-Lam site are W and SE, while those at FR-Aur are W, SE, and E. At FR-Aur, these prevailing directions are associated with better energy closure (> 0.8), while directions (S, SW) with fewer and weaker winds systematically have lower EBC (< 0.7). This strong wind dependence at FR-Aur is due to the high wind speeds (~2.6 m s^{-1}) experienced at this site, which are further strengthened by the gentle slope that encourages the development of turbulence and instability. The statistical indicators obtained in this study are comparable to those reported for sites with similar climatic conditions (Eshonkulov et al., 2019), and in Xin et al. (2018). For example, Xin et al. (2018) classified the flux data of 10 study sites into 16 wind directions, and observed higher closure (> 0.7) for the dominant wind direction, while closure (< 0.5) was lower for other sectors.

However, at FR-Lam, the closure for the 8 wind sectors for both the wheat and maize seasons was generally low and homogeneous, with values ranging between 0.52 and 0.75. This result is considered to be statistically significant since for each wind sector, the data set is largely representative (as indicated by the dot size). A thick surrounding forest shields the site, and this significantly decreases wind speeds, and dampens mechanical turbulence and turbulent transport (Giometto et al., 2017). On the contrary, the topography of FR-Aur which also corresponds to the main wind directions stimulates downslope flows creating larger turbulence.

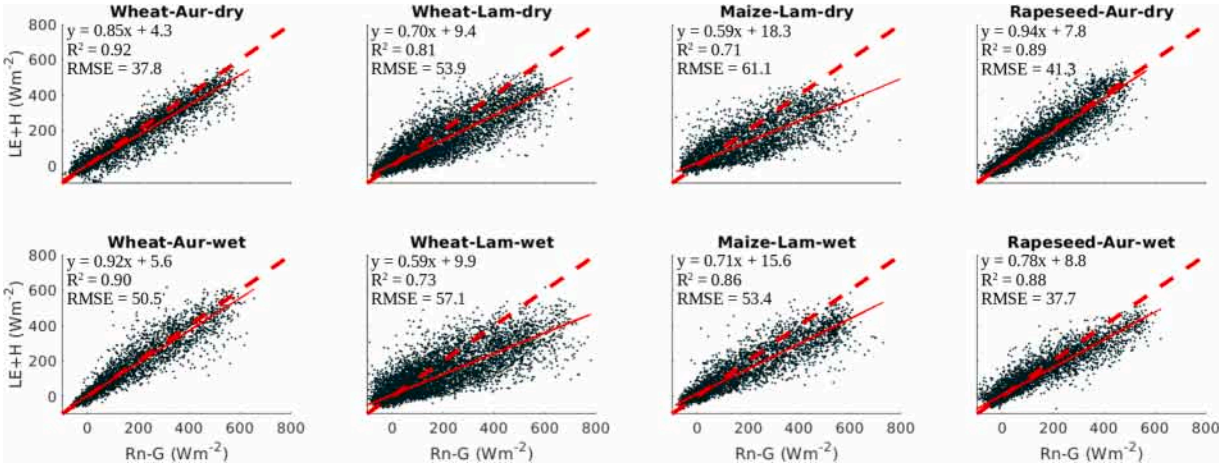

Fig. 3. Regression between (H+LE) and (Rn-G) at a half-hourly time step for the selected seasons (dry/wet, crop and site). The broken and solid black lines represent the 1:1 and the regression lines, respectively. The equations on the plot correspond to the linear fit, R2 is the coefficient of determination, and RMSE is presented in W m-2.

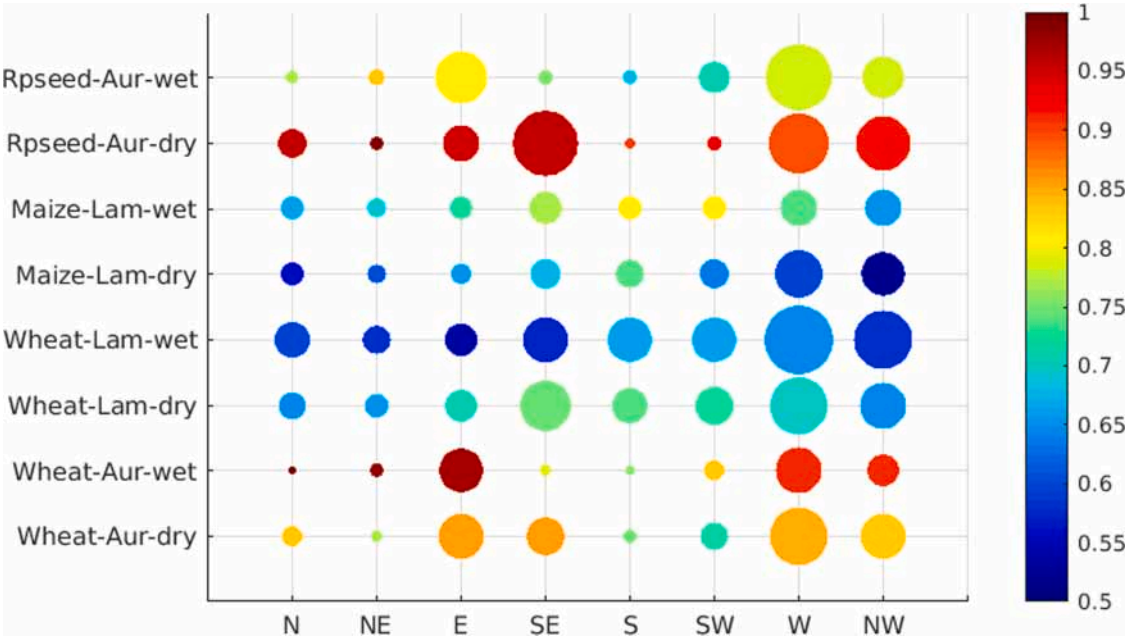

Fig. 4. Distribution of the EBC in terms of the wind direction for the different crop-seasons. High energy balance closure (close to 1) is presented in red; blue indicates weak closure. The dot size represents the number of data points.

3.2.2. Friction velocity

Fig. 5a shows the mean monthly plot of the turbulent parameter (friction velocity u^*) obtained from the sonic anemometer between 2005 and 2016 at both sites. This figure reveals that the turbulent exchange of momentum within the atmosphere-vegetation-soil continuum was stronger at FR-Aur than at FR-Lam. This was particularly obvious during summer (May and June) when FR-Aur and FR-Lam accommodated winter crops (wheat or rapeseed) and summer crops (maize), respectively. As shown by Franssen et al. (2010), higher u^* values are often associated with higher average net radiation. This fits well with the results at both sites.

Fig. 5b shows the effect of u^* on the closure of the contrasting crop-seasons. A threshold value that placed the u^* values in the low or high category (0.15 m s^{-1} at FR-Lam and 0.2 m s^{-1} at FR-Aur) was determined as the median of the u^* distribution. At both sites, high u^* globally increased the EBC by ~7% for both the dry and wet seasons as similarly reported in Franssen et al. (2010) and Xin et al. (2018). Franssen et al. (2010) obtained a linear relationship between the energy balance closure and u^*, while Xin et al. (2018) reported a single peak relationship with the energy balance ratio (EBR) peaking for u^* between 0.20 and 0.25 m s^{-1}. However, this may be linked to the seasonal effect of increasing u^* with stronger net radiation, as the phenological stage is not accounted for in Fig. 5b. However, this stability indicator played no significant role in the closure observed in maize whose growing season is shorter.

One can also attribute this difference in u^* values between both sites during summer (higher in FR-Aur, and lower in FR-Lam) to the lower wind velocities observed at FR-Lam especially during the

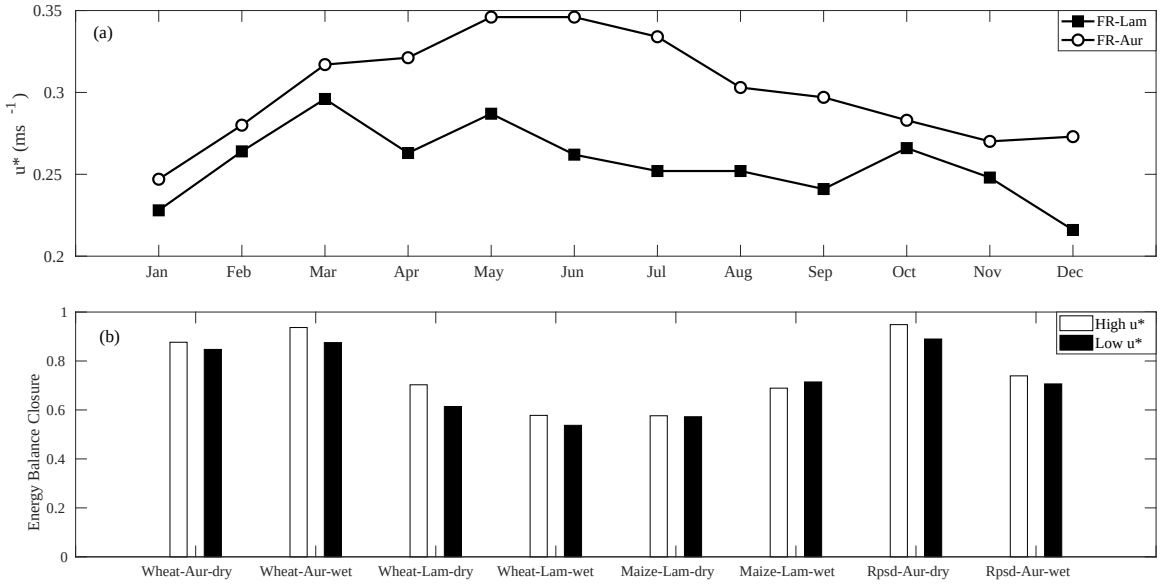

Fig. 5. (a) Monthly mean values of the friction velocity for FR-Lam (square) and FR-Aur (circle); (b) Impact of friction velocity on the EBC for the contrasting crop seasons.

maize season

3.2.3. Atmospheric stability

The effect of buoyancy is to increase turbulence, and intensify atmospheric mixing. The stability parameter $\varsigma = z/L$ was used to characterize the atmospheric state, where z is the measurement height of the anemometer, and L is the Obukhov length (Mahrt et al., 1998). This stability parameter corresponds to the ratio of buoyancy suppression to shear production under equivalent neutral conditions. |L| is the height above the ground where the buoyancy and shear production of turbulent kinetic energy (TKE) are of equal magnitude. Below this height, shear dominates, and above it, buoyancy dominates. With equal representation of each regime (similar dot size), flux measurements of the selected crops were classified using three stability regimes: $z/L \leq -0.1$ (unstable condition), $-0.1 < z/L < 0.1$ (neutral condition), and $z/L \geq 0.1$ (stable condition). The response of the energy closure of each class is shown in Fig. 6. The most pronounced difference was the transition of a stable condition (0.5) to a neutral atmospheric condition (0.7), while a minute improvement was observed in the EBC during the transition from the neutral to unstable state.

Fig. 5 and Fig. 6 distinctly reveal that FR-Aur benefits from stronger turbulence. This turbulence is generated by two effects: mechanical shear of the wind over rough surfaces, and convection due to higher surface temperature than in the air above. As u* and z/L are related to momentum, they are indicators of the mechanical turbulence for the three atmospheric stability conditions (Eshonkulov et al., 2019). As a result, both parameters favor the production of high frequency fluxes. The relevance of these parameters to energy closure has been noted in several studies (Franssen et al., 2010; Fratini and Mauder, 2014), and these are in agreement with our results. They usually invoke that the conditions of Taylor's hypothesis (the temporal average replaces spatial average) are better fulfilled with high u^* and unstable surface layer. However, at FR-Lam, despite the flat and homogeneous topography, the closure remains low, and this could be attributed to: (1) weaker turbulence, the non-turbulent advective fluxes are missed; (2) turbulent structures with time scales larger than the averaging time are uncaptured.

3.3. Dependency of SEB on crop phenological stages and rainfall

*3.3.1. Effect of the plant functioning on the **SEB** and its partitioning*

Fig. 7. shows the mean EBC with its corresponding mean residuals in W m^{-2} according to the crop stage and rainfall conditions. Again, larger and highly variable EBC (0.60 to 0.89) with smaller residuals was observed at FR-Aur, while FR-Lam exhibited more stability (0.50 to 0.62) across the crop stages.

Energy closure and residual energy increased as low crops transitioned into developed crops for most winter crops, except rapeseed-Aur-wet and wheat-Aur-wet. This behavior could be a result of seasonality effect where a low vegetation period occurred during winter, a season associated with low fluxes, while the period of developed crops (April to June) corresponds to stronger convective fluxes that increases the potential of the energy closure. A similar observation was made in Wilson et al. (2002); a lower closure (0.72) was reported for winter seasons, and a higher closure for summer periods (0.81). This low closure (in low crops) and high closure (in developed crops) was also reported in Imukova et al. (2016) in the experimental analysis performed on some winter wheat stands in Kraichgau, Germany, where towards the end of the growing season, an increase in EBC was observed.

To complete the analysis, Fig. 8 shows the distribution of energy fluxes (normalized by *Rn*) by crop type and phenological stages. Each flux exhibits similar dynamics for the same crop type, with very strong variability between crop stages, while each energy component behaved uniquely. For the different crop types, *LE* constituted an average of 29% of *Rn* for low crops, 41% for developed crops, 25% during senescence, 19% for post-harvest, and 22% over bare soils; while for the sensible heat flux, 22%, 22%, 42%, 36, and 37% of *Rn* was partitioned during these crop stages respectively. The parabolic behavior of the ground heat flux was essentially regulated by the magnitude of *Rn* and canopy structure. Thus, over low crops, *G* accounted for 30% of *Rn*, dropping to 16% during peak growth, and further during senescence (13%).

Besides, closure was higher during the bare soil period that succeeded the residue-covered postharvest phase with an EBC increase of 11%, 24%, 1%, 4.7%, and 9% (with respective imbalance difference of 57 W m^{-2}, 20 W m^{-2}, 37 W m^{-2}, 1 W m^{-2}, and 59 W m^{-2}) in wheat-Aur-dry, wheat-Lam-dry, wheat-Lam-wet, rapeseed-Aur-dry, and rapeseed-Aur-wet respectively. This suggests that the presence of harvest residues plays an important role in the SEB. According to Fig. 8, the ratio *G/Rn* is usually larger during the bare soil phase (~17%) following

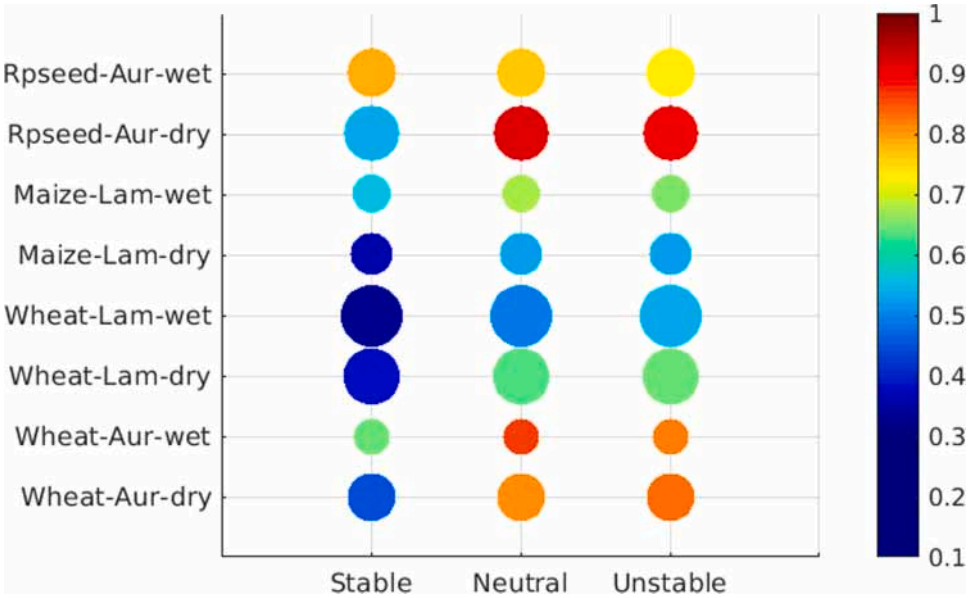

Fig. 6. Variability of the EBC for the 3 regimes of atmospheric stability (stable: $z/L \geq 0.1$; neutral: $-0.1 < z/L < 0.1$; unstable: $z/L \leq -0.1$).

post-harvest, except at FR-Lam where there's a longer presence of wheat residue (~3months). This specific case makes it difficult to separate the seasonality effect from the residue's effect. Conversely, in maize, *G/Rn* over the bare-soil and post-harvest period are not very different because of the absence of residues after harvest. Further analysis of the residue's impact on *G* revealed that over the crop seasons in FR-Aur (with the exception of wheat-Aur-wet due to unavailable data), the maximum mean value for *G* varied from 80 W m^{-2} during post-harvest period to 104 W m^{-2} during the bare soil period (see S3 in supplementary file). The least variability is observed in rapeseed-Aur-dry due to the thin residue layer. This behavior has been aptly described by Horton et al. (1996), and Chung and Horton (1987): residues act as a thermal insulator with two effects: (1) reduces the solar radiation absorbed by the soil due to the high reflectivity of the residues, and (2) their thermal conductivity is lower.

Across other crop seasons, no systematic pattern of the EBC in relation to crop stages was observed (Fig. 7). At certain times, EBC was higher with higher vegetation, and residual energy decreased (wheat-Aur-dry and maize-Lam-dry), while at other times, EBC was lower for developed crops accompanied by larger residual energy (maize-Lam-wet and rapeseed-Aur-wet).

The leaf area index modulates turbulent transfers and radiation absorption, hence, developed crops (high LAI) intercept incoming radiation, which decreases the amount of energy absorbed by the surface. Hammerle et al. (2008) demonstrated this experimentally over Stubai valley in Austria, and reported that *G* accounted for ~25% of *Rn* during periods with low foliage cover and much less under a dense canopy. Similarly, Santanello and Friedl (2003) found that *G* was usually less than 10% of *Rn* over thick canopies. In addition, the presence of vegetation resulted in higher *LE/Rn* due to increased transpiration (Heilman et al., 1994; Wohlfahrt et al., 2001; O'Brien et al., 2018), which dropped by 48% during senescence as transpiring leaves and stems started discoloring except in rapeseed-Aur-wet.

Furthermore, a role reversal was observed between the dry and wet seasons at FR-Aur. For low and developed crops of wheat-Aur and rapeseed-Aur, more energy was partitioned into *G* for wet seasons, while for subsequent crop stages, *G* was higher in the dry seasons than in the wet seasons. Periods with higher *G* values were characterized by higher rainfall amounts with differences of 200 mm (for low rapeseed), 45 mm (for developed rapeseed), 95 mm (for senescent rapeseed), 155 mm (for low wheat at Aur), and 21 mm (for developed wheat at Aur). Analysis revealed that *G* was regulated by high rainfall, and the resulting soil moisture stimulates an increase in thermal conductivity, a reduction in soil albedo, and consequently an increase in energy absorption. This behavior was not observed for wheat-Lam, although the rainfall recorded for the developed crop in the wet year was 200 mm higher than that of the dry year. In summary, with an *LAI* peaking at 5.4 m^2 m^{-2}, the shading effect that the canopy of wheat-Lam-wet provided masked the positive effect that a high soil thermal conductivity could contribute to *G*. Thus, the magnitude of *G* for wheat-Lam-dry and wheat-Lam-wet were comparable over developed vegetation.

Strong sensible heat fluxes ranging between 20 and 56% of the net radiation was observed across all the crop stages in rapeseed. In contrast, only 13–30% of *Rn* was partitioned into *H* in maize, and this was compensated for by *LE*. Of great interest is the scatter between the dry and the wet seasons especially for rapeseed during senescence. During this stage, *LE* and *H* clearly exhibited opposite behaviors. *LE* accounted for 40% of *Rn* (in the wet year) and 18% of *Rn* (in the dry year), while *H* had a weaker magnitude of 27% of *Rn* in the wet year and 56% of *Rn* in the dry year.

In conclusion, the site effect takes precedence over the crop type; both the turbulent and conduction fluxes are higher at FR-Aur compared to FR-Lam (Fig. 8) even for the same crop type. Nevertheless, on a given site, we frequently find certain energy balance trends related to the surface state/vegetation stage, e.g., a better closure when comparing bare-soil periods to post-harvest periods, or when the vegetation is well developed rather than low.

3.3.2. *Effect of rainfall*

Fig. 9 shows the mean EBC according to each crop stage with the corresponding cumulative rainfall (+ irrigation). FR-Lam has higher values of SWC than FR-Aur due to the difference in soil texture. As a result of its higher clay content (> 50%), FR-Lam has a higher water holding capacity for the same amount of water supply (Dare-Idowu et al., 2021). Similarly, shallower water table and large puddles of water are regularly observed on this plot during winter and spring. In contrast, the openness, windiness, and steepness of FR-Aur make it susceptible to quick drying, evaporation, and run-off, respectively.

For all crops at FR-Lam, the total cumulative rainfall was 564 mm, 693 mm, 338 mm, 447 mm for wheat-Lam-dry, wheat-Lam-wet, maize-Lam-dry, and maize-Lam-wet, respectively. Higher rainfall was recorded for low and developed crops compared to other stages, especially maize, due to the irrigation events that favored evapotranspiration fluxes and improved closure (see Fig. 8 and Fig. 9.

For wheat-Aur-dry and rapeseed-Aur-dry, the closure over the developed vegetation was 19% and 22%, respectively, higher than that of the low crops. Here, seasonality played a major role because even though rainfall was at least 100 mm during the developed stages. The atmospheric demand ($T_a > 12$ °C & $RH < 80\%$) was higher than that of low crops ($T_a < 5$ °C & $RH > 86\%$), in addition to a noticeable high sensible heat flux for developed rapeseed (Fig. 8).

In contrast, over wheat-Aur-wet and rapeseed-Aur-wet, rainfall was 82 mm and 165 mm higher, respectively, for low crops. The lower closure observed in the developed stages of the aforementioned crops can be related to the low wind velocities that prevailed during this period. For wheat-Aur-wet and rapeseed-Aur-wet, we observed wind velocities which were 29% and 8% lower respectively, during the developed crop than the low crop phases.

There were no data for the postharvest and bare-soil periods for wheat-Aur-wet. Nevertheless, EBC was highest for the wet crop-season (0.92) with $P = 580$ mm compared with the dry year (0.85) with $P = 415$ mm, as shown in Fig. 3.

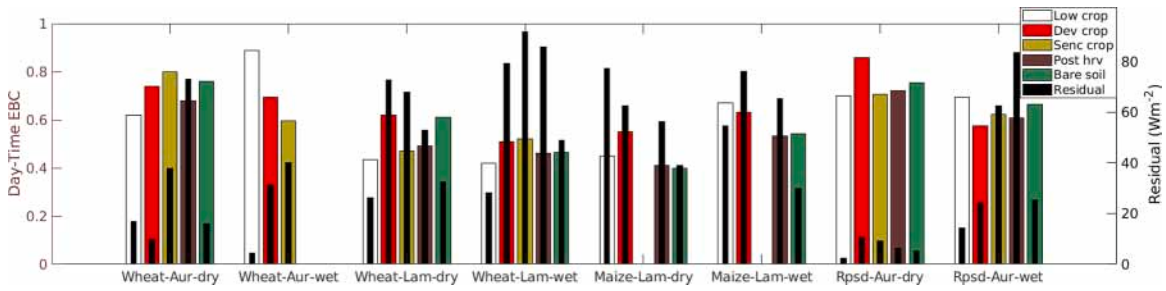

Fig. 7. Daytime EBC (colored bars) and the corresponding residual (black bars) for the crop stages of the contrasting seasons. The different colors correspond to the different surface states: white corresponds to the low crops, red to developed crops, yellow corresponds to the senescent crop, while brown and green correspond to the post harvest and bare soil periods respectively. Finally, the black bars indicate the residual energy, to be read on the right-hand axis.

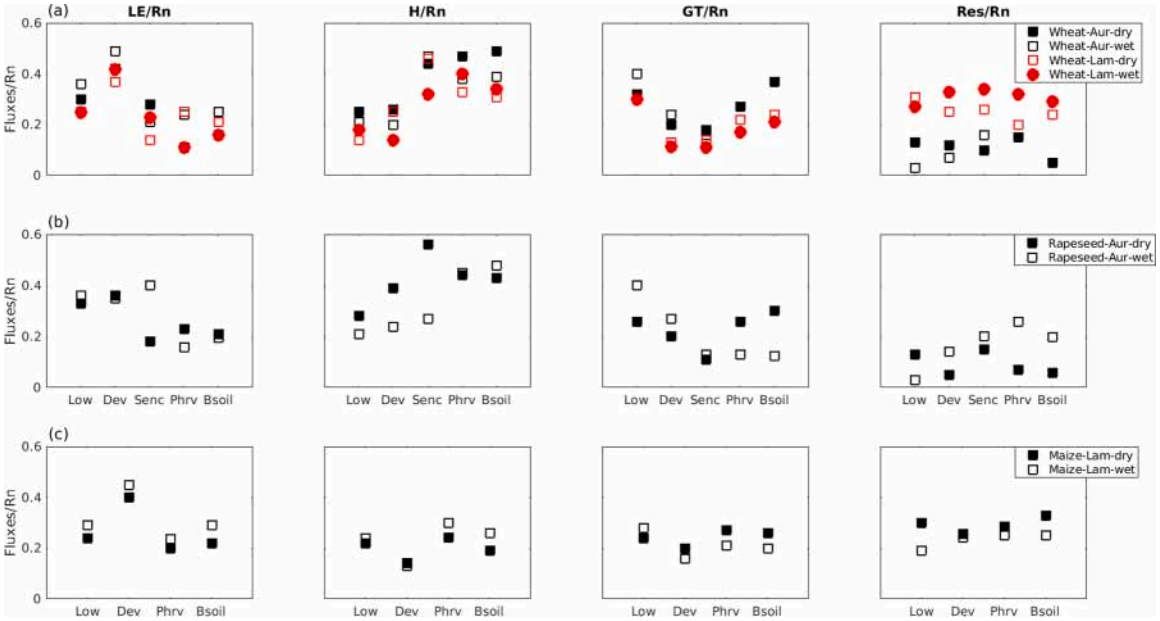

Fig. 8. Variability of the energy fluxes normalized by net radiation according to each crop stage of (a) wheat at the FR-Lam and FR-Aur site; (b) rapeseed at FR-Aur; (c) maize at FR-Lam.

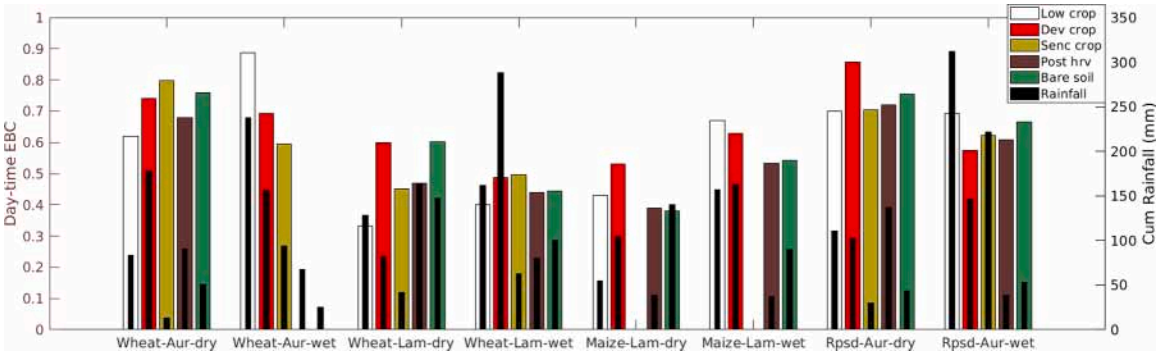

Fig. 9. Daytime energy balance closure (colored bars) for the different crop stages with cumulative rainfall (black bars).

3.4. *Effect of advection on energy imbalance*

Fig. 10 (a and b) presents a temporal series of the sensible heat advection term (A_H) and residual energy (*Res*) computed from 2006 to 2015 between 10h30 and 12h00 for both sites. At FR-Lam, A_H oscillated between 20 and 180 W m^{-2}, exhibited similar temporal dynamics as *Res,* and captured very closely the minimum and maximum values which is similar to the observation of V. García-Santos et al. (2018). At FR-Aur, a similar trend but with a lower magnitude that ranged between 3 and 98 W m^{-2} was observed.

Essentially, advection is mainly induced by topography, land use, and farm practices such as irrigation, etc. Fig. 10 shows that advection was of immense magnitude at FR-Lam, thus explaining the low energy balance closure observed at this site when only the traditional energy balance terms including S_G were considered. FR-Lam is a topographically flat site but with thick forest surrounding the plot. The edge of the forest is more than 200 m from the EC tower in its closest direction, which is a generally acceptable distance to ensure the representation of the turbulent fluxes. This leads to a heterogeneous surface temperature distribution. This analysis agrees well with the study of Xin et al. (2018), who reported low EBR over 4 flat terrains on the Tibetan Plateau due to the presence and influence of the buildings close to the sites.

Another heterogeneity-inducing factor is irrigation; FR-Lam is frequently irrigated to supplement rainfall, while FR-Aur is never irrigated. In addition, irrigation period often lasts for several days which increases the heterogeneity between the already-irrigated areas, and the yet-to-be-irrigated areas; as similarly discovered in the experimental study of Xu et al. (2017). They recorded low EBRs (~0.6) during these heterogeneous periods, which increased (> 0.8) after achieving a certain level of uniform wetness. At FR-Aur, heterogeneity introduced by topography played a minute role contrary to FR-Lam where EBC and A_H remained low and high, respectively. This stresses the role of agricultural practices and surrounding structures on the SEB as revealed in Panin et al. (1998) and Finnigan et al. (2003).

On the other hand, over FR-Aur, weaker magnitude of advection was found, as already verified by its high EBC. Heterogeneity-inducing practices and structures are absent at this site, and the slope corresponds to the main wind direction which minimizes the existence of thermally induced secondary circulations.

On average, A_H accounted for 57% and 60% of the estimated imbalance at FR-Lam and FR-Aur, respectively, leaving the energy budget unclosed. Oncley et al. (2007) made a comparable observation although over an irrigated cotton field in which during certain periods of their study, A_H could not explain the energy imbalance. This undoubtedly suggests the presence of some unaccounted-for energy sinks, and unidentified energy exchange processes (Stoy et al., 2013; Mauder et al., 2020). One could be the advective transport of water vapor (latent heat advection), which although not considered in this study (due to its

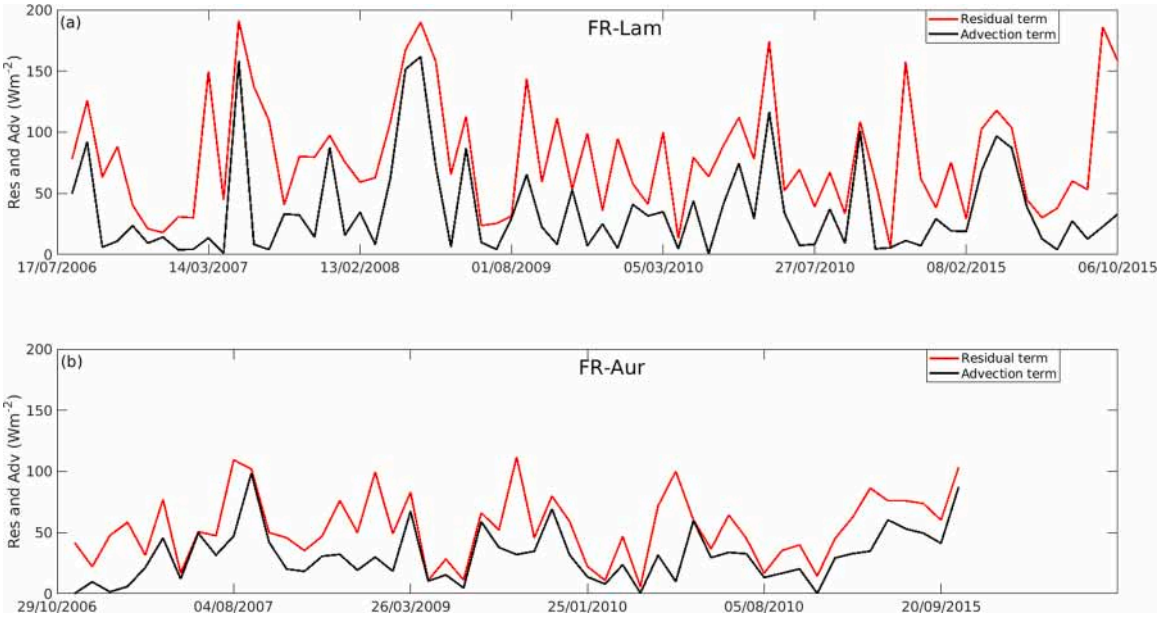

Fig. 10. Comparison of the residual energy with the order of magnitude of the estimated sensible heat advection term calculated in W m^{-2} from 2006 to 2015 at (a) FR-Lam and (b) FR-Aur.

complex instrumentation) could be as significant as the order of the evapotranspiration term if we refer to the experimental study of Simó et al. (2019) that was carried out over the UIB campus, Spain. However, for well-watered soils with adequate rainfall as in FR-Aur and FR-Lam, lower magnitude is expected due to the 'not very dry' atmosphere as in UIB. However, we hypothesize that this process would have a more substantial magnitude in FR-Lam than in FR-Aur given the frequent presence of water puddles in FR-Lam especially in winter and spring. In addition, the intermittent irrigation episodes in FR-Lam would encourage these evaporative transfers.

3.5. *Effect of time averaging*

Another factor that is linked to the unclosed energy budget is the uncaptured secondary structures (Laubach and Teichmann, 1999). These structures are large-scale fluxes whose slow motion can make the typical 30-min averaging time insufficient to resolve the large eddies depending on the local landscape (heterogeneity), and measurement

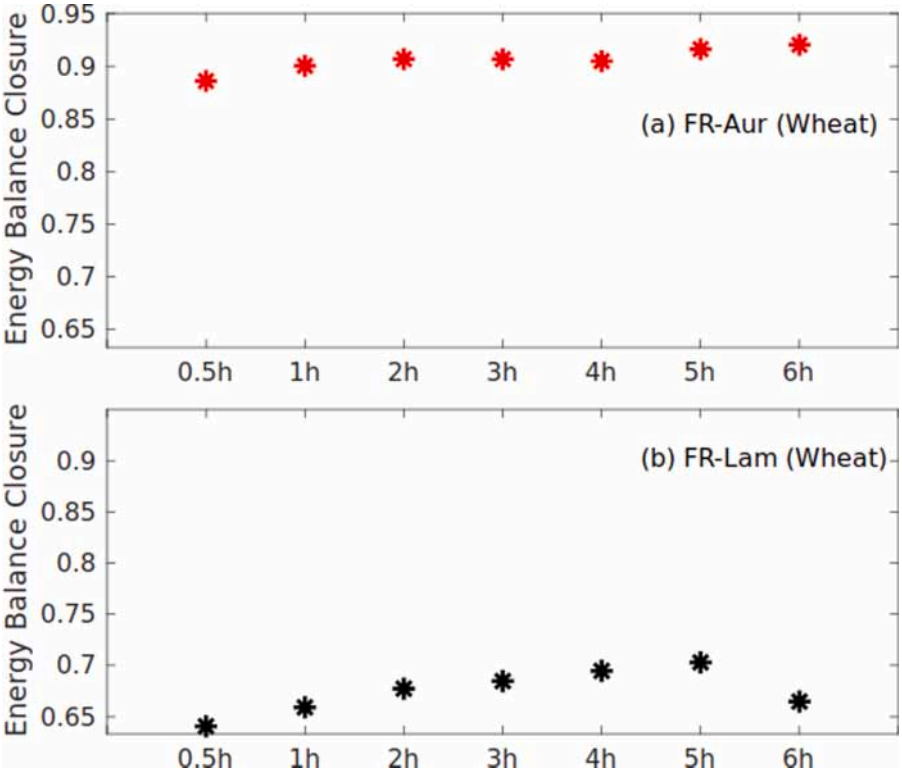

Fig. 11. The energy balance closure at different temporal scales for winter wheat at FR-Lam and FR-Aur.

height. To discuss the role of low-frequency processes (i.e. structures at few kms) in the surface energy balance, a rather simple approach was used. It involves estimating the EBC with surface fluxes averaged over different periods. An analysis carried out over four wheat seasons in FR-Lam and FR-Aur (see Fig. 11) revealed that an extension of the averaging time from 30 min to 6 h only slightly improved the energy balance closure by ~3.7%. This indicates that a large proportion of the low frequency fluxes have been adequately captured by the eddy covariance method during these wheat seasons. This is in agreement with the findings of Charuchittipan et al. (2014) who suggests that the 30 min averaging time is largely sufficient especially over low vegetation. Also, according to Charuchittipan et al. (2014), for taller vegetation such as maize in this study, an extension of the averaging time is recommended to include the contributions from the low frequency eddies.

Interestingly enough, considering time scales larger than 6 h (e.g. over the day) further improved the EBC. Nevertheless, as there are no boundary-layer processes with time scales longer than a few hours, compensation effects of the storage terms should appear, and may explain this improvement. Indeed, the energy stored in the morning is locally released in the afternoon and late evening (Foken, 2008). This is also in agreement with the study of Leuning et al. (2012) on the La Thuile dataset.

4. Conclusions

This study analyzed EC measurements and remotely sensed data for two dynamic agricultural systems (FR-Lam and FR-Aur) with similar environmental conditions in order to understand the energy closure, its controlling factors, and the factors that modulate flux partitioning. Emphasis was placed on comparing crop seasons with contrasting rainfall conditions. On average, closure was better in FR-Aur (82%), while only 67% of available energy was detected in FR-Lam. Energy closure at FR-Aur improves from 60% (stable atmospheric conditions) to 82% (high atmospheric instability). However, this intense instability is absent at FR-Lam, whose maximum EBC was 0.7 during its most unstable period.

Further analysis revealed that each site has a unique, and a significant influence on the energy closure, which is stronger than the impact introduced by the different crop types. In addition, the estimated sensible heat advection term is a significant contributor to energy imbalance with larger magnitudes at FR-Lam, in agreement with the plot's situation and activities.

In future studies, it would be interesting to account for the horizontal exchange of surface humidity advection which might be a pathway to further narrow the energy imbalance at these sites.Also, a study involving the comparison of a tropical climate and an arid climate (with the same crop type) is strongly recommended for future work. This study has provided us with key elements for land surface model validation in an ongoing study in which the upcoming companion paper would evaluate the soil-water budget during some maize seasons.

Author contributions

DO analyzed the data, the results, and wrote most of the paper. AB processed the data, analyzed the results, and contributed immensely in the writing. LJ also analyzed the results; JC formulated the objectives, the advection estimation, and contributed in the interpretation of the results. VR provided and processed the Landsat images and processing scripts. TT processed FR-Aur data and calculated the uncertainties of the EC measurements. All authors contributed to the revision of the paper.

Declaration of Competing Interest

The authors declare that they have no known competing financial interests or personal relationships that could have appeared to influence the work reported in this paper.

Acknowledgments

Oluwakemi's Ph.D. is being funded by the Petroleum Technology Development Fund (Grant No. OPD6018). Data acquisition for FR-Lam and FR-Aur was funded by the Institut National des Sciences de l'Univers of the centre National de la Recherche Scientifique through ICOS and OSR SW observatories. Facilities and staff were also funded by the University of Paul Sabatier, CNES and Institut de Recherche pour le Développement). Gratitude is extended to Franck Granouillac, Nicole Claverie, Bernard Marciel and Pascal Keravec for their technical support and assistance in the field. Special thanks are extended to Mr. Andréoni (farmer) and Ecole d'Ingénieur de Purpan for accommodating our measuring devices at FR-Aur and FR-Lam, respectively.

Supplementary materials

Supplementary material associated with this article can be found, in the online version, at doi:10.1016/j.agrformet.2021.108529.

References

Aubinet, M., Vesala, T., Papale, D., 2012. Eddy covariance: a Practical Guide to Measurement and Data Analysis. Springer, Dordrecht. https://doi.org/10.1007/978-94-007-2351-1.

Bagayoko, F., Yonkeu, S., Van de Giesen, N., 2006. Energy balance closure and footprint analysis using Eddy Covariance measurements in Eastern Burkina Faso. West Africa. Hydrology and Earth System Sciences Discussions. 3 https://doi.org/10.5194/hessd-3-2789-2006.

Baldocchi, D.D., 1994. A comparative study of mass and energy exchange over a closed C3 (wheat) and an open C4 (corn) canopy: the partitioning of available energy into latent and sensible heat exchange. Agric. For. Meteorol. 67, 191–220. https://doi.org/10.1016/0168-1923(94)90003-5.

Béziat, P., Rivalland, V., Jarosz, N., Ceschia, Eric., Boulet, G., Gentine, P., 2009. Crop evapotranspiration partitioning and comparison of different water use efficiency approaches.

Burba, G., Anderson, D., 2007. Introduction to the Eddy Covariance Method: general Guidelines and Conventional Workflow. https://doi.org/10.13140/RG.2.1.3723.5683.

Campbell, G.S., Norman, J.M., 1998. An Introduction to Environmental Biophysics, 2nd ed. Springer-Verlag, New York, p. 286.

Charuchittipan, D., Babel, W., Mauder, M., Leps, J., Foken, T., 2014. Extension of the Averaging Time in Eddy-Covariance Measurements and Its Effect on the Energy Balance Closure. Boundary Layer Meteorol 152, 303–327. https://doi.org/10.1007/s10546-014-9922-6.

Chung, S.O., Horton, R., 1987. Soil heat and water flow with a partial surface mulch. Water Resour. Res. 23 (12), 2175–2186. https://doi.org/10.1029/WR023i012p02175.

Culf, A.D., Foken, T., Gash, J.H.C., et al., 2004. The Energy Balance Closure Problem. In: Kabat, P., et al. (Eds.), Vegetation, Water, Humans and the Climate. Global Change -The IGBP Series. Springer, Berlin, Heidelberg, pp. 159–166. https://doi.org/10.1007/978-3-642-18948-7_13.

Cuxart, J., Conangla, L., Jiménez, M.A., 2015. Evaluation of the surface energy budget equation with experimental data and the ECMWF model in the Ebro Valley. J. Geophys. Res. Atmos. 120, 1008–1022. https://doi.org/10.1002/2014JD022296.

Cuxart, J., Wrenger, B., Martínez-Villagrasa, D., Reuder, J., Jonassen, M.O., Jiménez, M. A., Lothon, M., Lohou, F., Hartogensis, O., Dünnermann, J., Conangla, L., Garai, A., 2016. Estimation of the advection effects induced by surface heterogeneities in the surface energy budget. Atmos. Chem. Phys. 16, 9489–9504. https://doi.org/10.5194/acp-16-9489-2016.

Dare-Idowu, O., Jarlan, L., Le-Dantec, V., Rivalland, V., Ceschia, E., Boone, A., Brut, A., 2021. Hydrological Functioning of Maize Crops in Southwest France Using Eddy Covariance Measurements and a Land Surface Model. Water 2021 13, 1481. https://doi.org/10.3390/w13111481.

Eshonkulov, R., Poyda, A., Ingwersen, J., Wizemann, H., Weber, T., Kremer, P., Högy, P., Pulatov, A., Streck, T., 2019. Evaluating multi-year, multi-site data on the energy balance closure of eddy-covariance flux measurements at cropland sites in southwestern Germany. Biogeosciences 16. https://doi.org/10.5194/bg-16-521-2019.

Field, R.T., Fritschen, L.J., Kanemasu, E.T., Smith, E.A., Stewart, J.B., Verma, S.B., Kustas, W.P., 1992. Calibration, comparison, and correction of net radiometer instruments used during FIFE. J. Geophys. Res. D: Atmos. 97, 18681–18695. https://doi.org/10.1029/91JD03171.

Finnigan, J.J., Clement, R., Malhi, Y., Leuning, R., Cleugh, H.A., 2003. A re-evaluation of long-term flux measurement techniques, part I: averaging and coordinate rotation. Boundary Layer Meteorol 107, 1–48. https://doi.org/10.1023/A:1021554900225.

Foken, T., Oncley, S, 1995. Workshop on Instrumental and Methodical Problems of Land Surface Flux Measurements. Bulletin of the American Meteorological Society 76 (7), 1191–1224. https://doi.org/10.1175/1520-0477-76.7.1191.

Foken, T., Wichura, B., 1996. Tools for quality assessment of surface-based flux measurements. Agr. For. Meteorol 78 (1–2), 83–105. https://doi.org/10.1016/0168-1923(95)02248-1.
Foken, T., 2008. The Energy Balance Closure Problem: an Overview. Ecological Applications 18, 1351–1367. https://doi.org/10.1890/06-0922.1.
Foken, T., Mauder, M., Liebethal, C., Wimmer, F., Beyrich, F., Leps, J.P., Raasch, S., DeBruin, H., Meijninger, W., Bange, J., 2010. Energy balance closure for the LITFASS-2003 experiment. Theor Appl Climatol 101, 149–160. https://doi.org/10.1007/s00704-009-0216-8.
Franssen, H., Stöckli, R., Lehner, I., Rotenberg, E., Seneviratne, S., 2010. Energy balance closure of eddy-covariance data: a multi-site analysis for European FLUXNET stations. Agric. For. Meteorol. 150, 1553–1567. https://doi.org/10.1016/j.agrformet.2010.08.005.
Fratini, G., Mauder, M., 2014. Towards a consistent eddy-covariance processing: an intercomparison of EddyPro and TK3. Atmospheric Measurement Techniques Discussions. 7, 2107–2126. https://doi.org/10.5194/amt-7-2273-2014.
Gaillardet, J.I., Braud, F., Hankard, S., Anquetin, Olivier B., et al., 2018. OZCAR: the French Network of Critical Zone Observatories. Vadose Zone Journal. Soil science society of America - Geological society of America 17 (1), 1–24. https://doi.org/10.2136/vzj2018.04.0067.
Gao, Z., Liu, H., Katul, G., Foken, T., 2017. Non-closure of the surface energy balance explained by phase difference between vertical velocity and scalars of large atmospheric eddies. Environmental Research Letters 12. https://doi.org/10.1088/1748-9326/aa625b.
García-Santos, V., Cuxart, J., Jiménez, M., Villagrasa, D., Jiménez, M., Simó, G., Picos, R., Caselles, V., 2018. Study of Temperature Heterogeneities at Sub-Kilometric Scales and Influence on Surface–Atmosphere Energy Interactions. IEEE T. Geosci. Remote. 57, 640–654. https://doi.org/10.1109/TGRS.2018.2859182.
Giometto, M., Christen, A., Egli, P., Schmid, M.F., Tooke, R.T., Coops, N.C., Parlange, M., 2017. Effects of trees on mean wind, turbulence and momentum exchange within and above a real urban environment. Adv. Water Res. https://doi.org/10.1016/j.advwatres.2017.06.018.
Hammerle, A., Haslwanter, A., Tappeiner, U., Cernusca, A., Wohlfahrt, G., 2008. Leaf area controls on energy partitioning of a temperate mountain grassland. Biogeosciences 5, 421–431. https://doi.org/10.5194/bg-5-421-2008.
Heilman, J.L., McInnes, K.J., Savage, M.J., Gesch, R.W., Lascano, R.J., 1994. Soil and canopy balances in a west Texas vineyard. Agric. For. Meteorol. 71, 99–114. https://doi.org/10.1016/0168-1923(94)90102-3.
Horton, R., Bristow, K.L., Kluitenberg, G.J., et al., 1996. Crop residue effects on surface radiation and energy balance - review. Theor. Appl. Climatol. 54, 27–37. https://doi.org/10.1007/BF00863556.
Imukova, K., Ingwersen, J., Hevart, M., Streck, T., 2016. Energy balance closure on a winter wheat stand: comparing the eddy covariance technique with the soil water balance method. Biogeosciences 13, 63–75. https://doi.org/10.5194/bg-13-63-2016.
Kljun, N., Calanca, P., Rotach, M., Schmid, H., 2004. A Simple Parameterisation for Flux Footprint Predictions. Boundary-Layer Meteorol. 112. 503–523. https://doi.org/10.1023/B:BOUN.0000030653.71031.96.
Kohsiek, W., Liebethal, C., Foken, T., Vogt, R., Oncley, S., Bernhofer, C., De Bruin, H., 2007. The Energy Balance Experiment EBEX-2000. Part III: behaviour and quality of the radiation measurements. Boundary-Layer Meteoro 123, 55–75. https://doi.org/10.1007/s10546-006-9135-8.
Laubach, J., Teichmann, U., 1999. Surface Energy Budget Variability: a Case Study over Grass with Special Regard to Minor Inhomogeneities in the Source Area. Theor. Appl. Climatol. 62, 9–24. https://doi.org/10.1007/s007040050070.
Leuning, R., Van Gorsela, E., Massman, W.J., Isaac, P.R., 2012. Reflections on the surface energy imbalance problem. Agric. For. Meteorol. 156, 65–74. https://doi.org/10.1016/j.agrformet.2011.12.002.
Mahrt, L., Sun, J., Blumen, W., Delany, T., Oncley, S., 1998. Nocturnal Boundary-Layer Regimes. Boundary-Layer Meteorology. 88. https://doi.org/10.1023/A:1001171313493.
Masseroni, D., Corbari, C., Mancini, M., 2014. Limitations and improvements of the energy balance closure with reference to experimental data measured over a maize field. Atmosphere (Basel) 27 (4), 335–352. https://doi.org/10.1016/S0187-6236(14)70033-5.
Mauder, M., Foken, T., Cuxart, J., 2020. Surface-Energy-Balance Closure over Land: a Review. Boundary-Layer Meteorology. https://doi.org/10.1007/s10546-020-00529-6.
McCaughy, J.H., Saxton, W.L., 1988. Energy balance storage terms in a mixed forest. Agric. For. Meteorol. 44, 1–18. https://doi.org/10.1016/0168-1923(88)90029-9.
Meyers, T.P., Hollinger, S.E., 2004. An assessment of storage terms in the surface energy balance of maize and soybean. Agric. For. Meteorol. 125, 105–115. https://doi.org/10.1016/j.agrformet.2004.03.001.
Moderow, U., Aubinet, M., Feigenwinter, C., et al., 2009. Available energy and energy balance closure at four coniferous forest sites across. Europe. Theor Appl Climatol 98, 397–412. https://doi.org/10.1007/s00704-009-0175-0.
Moore, C.J., 1986. Frequency response corrections for eddy correlation systems. Boundary-Layer Meteorol 37, 17–35. https://doi.org/10.1007/BF00122754.
Nobel, P.S., 1974. Introduction to Biophysical Plant Physiology. Freeman, New York.
Nordbo, A., Järvi, L., Vesala, T., 2012. Revised eddy covariance flux calculation methodologies – effect on urban energy balance. Tellus B 64. https://doi.org/10.3402/tellusb.v64i0.18184.
O'Brien, P.L., DeSutter, T.M., Casey, F.X.M., Daigh, A.L., Heitman, J.L., Derby, N.E., Khan, E., 2018. Daytime Surface Energy Fluxes over Soil Material Remediated Using Thermal Desorption. Agrosystems, Geosciences & Environment 1 (1–9), 180027. https://doi.org/10.2134/age2018.08.0027.
Oncley, S.P., Foken, T., Vogt, R., Kohsiek, W., DeBruin, H.A.R., Bernhofer, C., Christen, A., Van Gorsel, E., Grantz, D., Feigenwinter, C., Lehner, I., Liebethal, C., Liu, H., Mauder, M., Pitacco, A., Ribeiro, L., Weidinger, T., 2007. The energy balance experiment EBEX-2000. Part I: overview and energy balance. Boundary-Layer Meteorol 123, 1–28. https://doi.org/10.1007/s10546-007-9161-1.
Panin, G.N., Tetzlaff, G., Raabe, A., 1998. Inhomogeneity of the land surface and problems in the parameterization of surface fluxes in natural conditions. Theor Appl Climatol 60, 163–178. https://doi.org/10.1007/s007040050041.
Reichstein, M., Falge, E., Baldocchi, D., Papale, D., Aubinet, M., Berbigier, P., Bernhofer, C., Buchmann, N., Gilmanov, T., Granier, A., Grünwald, T., Havránková, K., Ilvesniemi, H., Janous, D., Knohl, A., Laurila, T., Lohila, A., Loustau, D., Matteucci, G., Valentini, R., 2005. On the Separation of Net Ecosystem Exchange into Assimilation and Ecosystem Respiration: review and Improved Algorithm. Glob. Change Biol. 11, 1424–1439. https://doi.org/10.1111/j.1365-2486.2005.001002.x.
Santanello, J., Friedl, M., 2003. Diurnal Covariation in Soil Heat Flux and Net Radiation. Journal of Applied Meteorology 42, 851–862. https://doi.org/10.1175/1520-0450,2003042%3C0851:DCISHF%3E2.0.CO;2.
Simó, G., Martínez-Villagrasa, D., Jiménez, M.A., Caselles, V., Cuxart, J., 2019. Impact of the Surface–Atmosphere Variables on the Relation Between Air and Land Surface Temperatures. In: Vilibić, I., Horvath, K., Palau, J. (Eds.), Meteorology and Climatology of the Mediterranean and Black Seas. Pageoph Topical Volumes. Birkhäuser. Cham. https://doi.org/10.1007/978-3-030-11958-4_13.
Stoy, P.C., Mauder, M., Foken, T., Marcolla, B., Boegh, E., Ibrom, A., Arain, M., Arneth, A., Aurela, M., Bernhofer, C., Cescatti, A., Dellwik, E., Duce, P., Gianelle, D., Gorsel, E., Kiely, G., Knohl, A., McCaughey, H., et al., 2013. A data-driven analysis of energy balance closure across FLUXNET research sites: the role of landscape-scale heterogeneity. Agric. For. Meteorol. 171 (172), 137–152. https://doi.org/10.1016/j.agrformet.2012.11.004.
Tardy, B., Rivalland, V., Huc, M., Hagolle, O., Marcq, S., Boulet, G., 2016. A Software Tool for Atmospheric Correction and Surface Temperature Estimation of Landsat Infrared Thermal Data. Remote Sens 8, 696. https://doi.org/10.3390/rs8090696.
Webb, E.K., Pearman, G.I., Leuning, R., 1980. Correction of flux measurements for density effects due to heat and water vapour transfer. Q.J.R. Meteorol. Soc. 106, 85–100. https://doi.org/10.1002/qj.49710644707, 9710644707" https://doi.org/10.1002/qj.49710644707.
Wilson, K., Goldstein, A., Falge, E., Aubinet, M., Baldocchi, D., Berbigier, P., Bernhofer, C., Ceulemans, R., Dolman, H., Field, C., Grelle, A., Ibrom, A., Law, B.E., Kowalski, A., Meyers, T., Moncrieff, J., Monson, R., Oechel, W., Tenhunen, J., Valentini, R., Verma, S., 2002. Energy balance closure at FLUXNET sites. Agric. For. Meteorol. 113, 223–243. https://doi.org/10.1016/S0168-1923(02)00109-0.
Wohlfahrt, G., Sapinsky, S., Tappeiner, U., Cernusca, A., 2001. Estimation of plant area index of grasslands from measurements of canopy radiation profiles. Agric. For. Meteorol. 109, 1–12. https://doi.org/10.1016/S0168-1923(01)00259-3.
Xin, Y.F., Chen, F., Zhao, P., Barlage, M., Blanken, P., Chen, Y.L., Chen, B., Wang, Y.J., 2018. Surface energy balance closure at ten sites over the Tibetan plateau. Agric. For. Meteorol. 259, 317–328. https://doi.org/10.1016/j.agrformet.2018.05.007.
Xu, Z., Ma, Y., Liu, S., Shi, W., Wang, J., 2017. Assessment of the Energy Balance Closure under Advective Conditions and Its Impact Using Remote Sensing Data. J. Appl. Meteor. Climatol. 56, 127–140. https://doi.org/10.1175/JAMC-D-16-0096.1.